

Heat Transfer Engineering

ISSN: (Print) (Online) Journal homepage: https://www.tandfonline.com/loi/uhte20

Numerical Study on Heat Transfer and Flow Characteristics of Supercritical CO_2 in Printed Circuit Heat Exchangers with Zigzag Channels

Qingqing Wang, Xin Huang, Bo Xu, Qiuxiang Chen & Haijun Wang

To cite this article: Qingqing Wang, Xin Huang, Bo Xu, Qiuxiang Chen & Haijun Wang (2023): Numerical Study on Heat Transfer and Flow Characteristics of Supercritical CO_2 in Printed Circuit Heat Exchangers with Zigzag Channels, Heat Transfer Engineering, DOI: 10.1080/01457632.2022.2164679

To link to this article: https://doi.org/10.1080/01457632.2022.2164679

Published online: 09 Jan 2023.

Submit your article to this journal

Article views: 82

View related articles

View Crossmark data

Full Terms & Conditions of access and use can be found at
https://www.tandfonline.com/action/journalInformation?journalCode=uhte20

HEAT TRANSFER ENGINEERING
https://doi.org/10.1080/01457632.2022.2164679

Taylor & Francis
Taylor & Francis Group

Check for updates

Numerical Study on Heat Transfer and Flow Characteristics of Supercritical CO_2 in Printed Circuit Heat Exchangers with Zigzag Channels

Qingqing Wang, Xin Huang, Bo Xu, Qiuxiang Chen, and Haijun Wang

State Key Laboratory of Multiphase Flow in Power Engineering, Xi'an Jiaotong University, Xi'an, Shaanxi, China

ABSTRACT

The heat transfer and flow characteristics of supercritical CO_2 in zigzag printed circuit heat exchangers (PCHEs) with different arcuate-sectional channels are numerically analyzed in this paper. The influences of channel width and bending angle of PCHE channels were discussed in detail. The upper side length of the arcuate channel ranges from 1.6 to 4.0 mm, and the bending angle varies from 15° to 25°. The inlet temperatures and pressures in cold side and hot side of PCHE are 373 K, 21 MPa and 493 K, 9 MPa, respectively. The mass flux in both sides of PCHE is equal, which ranging from 200 to 600 kg/m^2 s. The results show that the characteristics of heat transfer and flow in zigzag PCHEs are extremely complex, which are mainly related to the flow impact and separation in channels. In general, increasing channel width can enhance the heat transfer. In a certain mass flux and bending angle range, increasing the channel width appropriately can reduce the friction factor effectively. However, when the limit is exceeded, increasing the channel width will increase friction factor. Therefore, appropriate channel width and bending angle can simultaneously enhance heat transfer and reduce resistance, which has significance for the design optimization of PCHE structure.

Introduction

The emissions of greenhouse gases, especially CO_2, are considered to be one of the main causes of global warming, and traditional fossil power stations are major sources of CO_2. Developing environmentally friendly new power stations and improving energy efficiency are considered to be one of the effective ways to reduce CO_2 emissions. On this background, as a new type of power cycle, the supercritical CO_2 Brayton cycle has received more and more attention. Compared with water, CO_2 is also nontoxic and comes from a wide range of sources, but it has better compressibility, and its critical temperature and pressure are 304 K and 7.38 MPa, respectively. The supercritical CO_2 Brayton cycle makes full use of the high fluid density and low compression coefficient near the pseudocritical point, and the preferable stability in the supercritical region of supercritical CO_2 [1]. Therefore, the supercritical CO_2 Brayton cycle has the advantages of simple layout, compact structure and high efficiency [2], and it is considered to be the most promising power cycle for many new environmentally friendly power plants such as solar thermal power station, biomass power station, high temperature gas cooled reactor nuclear power station [3].

The recuperators and coolers are the largest components of the whole supercritical CO_2 Brayton cycle system [4]. Obviously, the design of heat exchanger has an appreciable impact on the performance and size of the cycle system. The traditional shell and tube heat exchangers cannot meet the economical and compact design requirements of the supercritical CO_2 Brayton cycle for its large volume and cost. Compared with the shell and tube heat exchangers, printed circuit heat exchangers (PCHEs) have the following advantages: (a) heat transfer area density reaches up to 2500 m^2/m^3; (b) capability to with stand high pressures reaches up to 60 MPa; (c) high compactness and simple structure [2, 5]. Hence, PCHEs are considered to be one of the best choices for heat exchangers in the supercritical CO_2 Brayton cycle [6]. PCHEs are plate-type compact heat exchangers in which flow channels are manufactured into the metal plates by photochemical etching method [7]. It has been reported several flow channels designs in PCHEs,

CONTACT Professor Haijun Wang whj@mail.xjtu.edu.cn State Key Laboratory of Multiphase Flow in Power Engineering, Xi'an Jiaotong University, Xi'an 710049, Shaanxi, China.

© 2023 Taylor & Francis Group, LLC

Nomenclature

A	area, m^2
A_c	cross-section area of PCHE channel, m^2
CFD	computational fluid dynamics
c_p	specific heat capacity, J/kg K
D_h	hydraulic diameter calculated, m
D_ω	cross-diffusion term, $kg/m^3\ s^2$
f	Fanning friction factor
g	gravity acceleration, m/s^2
G_k	production of turbulence kinetic energy, $kg/m\ s^3$
G_ω	production of specific dissipation rate, $kg/m^3\ s^2$
h	convective heat transfer coefficient, W/m^2 K
H	geometrical parameter of PCHE channel, m
H_e	enthalpy, J/kg
k	turbulent kinetic energy, m^2/s^2
L	geometrical parameter of PCHE channel, m
L_a	length of adiabatic section, m
L_α	flow length of channel, m
L_p	length of pitch, m
M	mass flux, kg/m^2 s
Nu	Nusselt number
P	wetted perimeter of PCHE channel, m
p	pressure, Pa
PCHE	printed circuit heat exchanger
Pr	Prandtl number, $Pr = \frac{c_p \mu}{\lambda}$
q	heat flux, W/m^2
r	geometrical parameter of PCHE channel, m
Re	Reynolds number, $Re = \frac{MD_h}{\mu}$
s	geometrical parameter of PCHE channel, m
SST	shear stress transfer
T	temperature, K
v	velocity, m/s
W	geometrical parameter of PCHE channel, m
X	physical quantities calculated by area-weighted average in Equation (8)
x, y, z	coordinate axes
Y_k	dissipation of turbulence kinetic energy, $kg/m\ s^3$ K
Y_ω	dissipation of specific dissipation rate, $kg/m\ s^3$ K
y^+	non-dimensional distance from wall

Greek symbols

α	bending angle, °
Γ_k	effective diffusivity of turbulence kinetic energy, Pa s
Γ_ω	effective diffusivity of specific dissipation rate, Pa s
Δp	pressure drop, Pa
ΔT	temperature difference, K
ρ	density, kg/m^3
μ	dynamic viscosity, Pa s
λ	thermal conductivity, W/m K
ω	specific dissipation rate, 1/s

Subscripts

b	bulk
cold	in the cold side of PCHE
correlation	empirical correlation
hot	in the hot side of PCHE
w	wall
t	turbulence
i, j, k	tensor indices

such as straight channels [8–10], zigzag channels [11–14], wave channels [15, 16], S-shape finned channels [17, 18], and airfoil finned channels [19–21]. Due to the dramatic change of thermal properties of supercritical CO_2, as well as the complex internal structure and various working conditions, the heat transfer and flow characteristics of PCHEs have attracted much attention.

In general, the flow channels in PCHEs can be divided into two categories: continuous and discontinuous channels. At present, there are relatively many studies on the heat transfer and flow characteristics of continuous channels. In addition, the hydraulic diameter of the PCHE channel is usually as 0.5–2 mm [22], it is difficult to obtain the details of internal flow and temperature field in PCHEs by experimental measurement. Therefore, computational fluid dynamics (CFD) method is often used to study the influence of PCHE channel structure on the flow and heat transfer. Zhang et al. [23] conducted numerical investigations on the coupled heat transfer of supercritical pressure CO_2 in a PCHE with straight semicircular channels, and the buoyancy effect on the local thermal performance is analyzed in detail. Saeed and Kim [24] numerically studied the effects of different fin angles on the thermal and hydraulic performance in a zigzag channel PCHE with supercritical CO_2. They found that with the increase of fin angle, the Nusselt number, frictional factor, and the performance evaluation criteria on both cold and hot sides decrease at different Reynolds numbers. de la Torre et al. [25] accomplished an optimization study of the zigzag channel PCHE with helium fluids by commercial software ANSYS CFX. In this research, they considered four geometric parameters: zigzag pitch length, zigzag angle, bend radius and zigzag phase-shift, and found that zigzag angle was the greatest influence on the heat transfer coefficient and the friction losses. Baik et al. [26] compared the hydraulic performance of zigzag PCHE with sharp corner channel and rounded corner channel by CFD method and found that the pressure drop of the sharp corner channel was 40–65% greater than that of the realistic rounded corner channel. Wen et al. [27] numerically calculated and compared the flow and heat transfer characteristics of supercritical CO_2 in PCHEs with sinusoidal and zigzag channels. It is found that the pressure drop of the inlet section contributed the most to the overall pressure drop in the sinusoidal and zigzag channels, and larger bend angles result in greater reductions in

pressure drop if sinusoidal channels are used instead of zigzag channels. Lee et al. [28] discussed the thermal hydraulic performance of the zigzag-type PCHEs with the inserted straight channels using numerical simulation method. The authors found that the heat transfer characteristics of the 0.5 and 1 mm straight channels are quite similar to those of the zigzag channel, but the pressure drops are less than that of the zigzag channel. Aneesh et al. [29] numerically studied thermo-hydraulic characteristics and performance of PCHEs with straight, triangular, sinusoidal, and trapezoidal periodic channels. It is found that the trapezoidal PCHE model offers the highest heat transfer and the thermal performance factor with the largest pressure drop. In all the above studies, the cross-section shape of the PCHE channels is the semicircle, which is the most common cross-sectional type. Through these studies, it can be found that these studies of PCHEs with continuous channels mainly focus on the thermal hydraulic performance effected by the change of flow direction structure.

However, there is no doubt that the structure of channel cross-section will affect the thermal hydraulic performance of PCHEs. Lee and Kim [30] compared the thermal hydraulic performance of zigzag PCHEs with semicircular, rectangular, trapezoidal, and circular cross-sectional channels. They found that rectangular channel cross-section showed the best thermal performance while the worst hydraulic performance under the same hydraulic diameter condition. Jeon et al. [31] numerically analyzed the thermal performance of cross flow PCHEs. It is found that the thermal performance of the PCHE decreases monotonically as the either of channel size increases, and the channel cross-sectional shape does not have significant effect on the thermal performance when the hydraulic diameter of the channels remains constant. Yang et al. [32] compared the heat transfer performance of wavy PCHEs with different narrow channels. They found that narrowing channel cross-section has a minor negative effect on the total heat transfer rate, and it will greatly reduce the volume of PCHE, but increase the pumping power. Lao et al. [33] numerically analyzed the heat transfer between supercritical CO_2 and molten salt in PCHE and found that the overall performance of PCHE is improved because the pressure drop of molten salt channel can be significantly reduced as the width of molten salt channel increased. The above studies revealed that the influence of the channel cross-section shape on the thermal hydraulic performance of PCHE with different axial structures is different under different working conditions. Therefore, it is necessary to further study the effect of channel cross-section on heat transfer and flow characteristics in order to provide support for the design optimization of PCHEs.

In this paper, a series of zigzag PCHE models with different arcuate-sectional channel widths and bending angles was established. The heat transfer and flow characteristics of supercritical CO_2 in zigzag PCHE are numerically analyzed in detail, and coupling effect of channel widths, bending angles and mass flux is emphasized.

Methodology

Physical model and boundary condition

Three-dimensional numerical calculation method was used in this study. The PCHE is manufactured by stacking and diffusion welding of metal plates with etching channels. In general, the heat transfer unit of PCHE has translational periodicity in geometric structure as the cross-section shown in Figure 1. To simplify the calculation, a hot channel and a cold channel are combined into a unit of heat transfer in this study. Periodic boundary conditions are used at the left, right, top, and bottom walls of the physical model as shown in Figure 2.

As shown in Figure 2, the zigzag channel PCHEs in this study are all counter flow heat exchangers, and the cold and hot channels have the same geometry. The flow directions of the hot and cold fluid are both along the z-axis, and the gravity is along the negative direction of y-axis. The entire channel can be divided into 8 periodic units which is named "pitch" along the flow direction. The bending angle of pitch is changed from 15° to 25°. In addition, adiabatic flow stabilization sections are added at the inlet and outlet

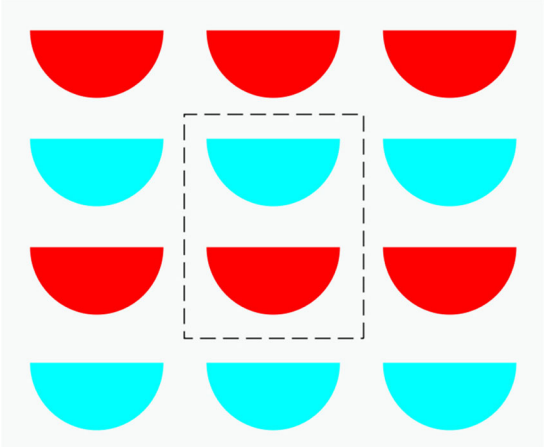


Figure 1. Cross-section of PCHE heat transfer unit.

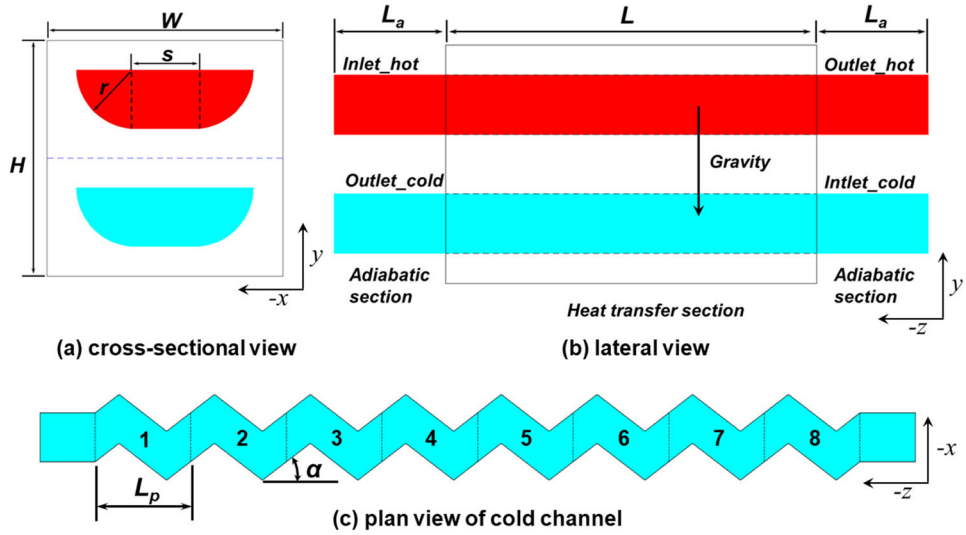


Figure 2. Physical model and dimension parameters of PCHE heat transfer unit.

Table 1. Geometric data of physical models.

Parameters	Numerical size
α	15°, 20°, 25°
H	3.2 mm
L	200 mm
L_a	20 mm
L_p	25 mm
r	0.8 mm
s	0 mm, 0.8 mm, 1.6 mm, 2.4 mm
W	$s + 2.4$ mm

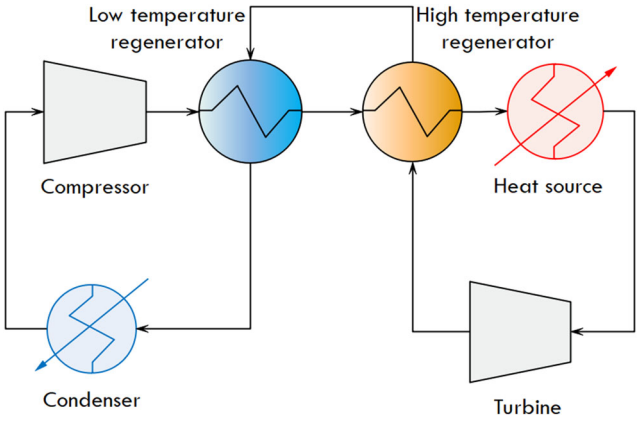


Figure 3. Simplified process flow diagram of supercritical CO_2 Brayton cycle.

of the heat exchange section. The cross-section shape of channel can be seen as a combination of two quarter circles and a rectangle, and the width of rectangle is changed from 0 to 2.4 mm. Varying the width of the rectangle produces a series of arcuate channel sections with different widths. Specific geometric parameters of PCHEs in this research are shown in Table 1.

Figure 3 shows a simplified process flow diagram of supercritical CO_2 Brayton cycle. The low temperature and high-pressure CO_2 flows through the cold sides of the regenerators and enters into the heat source. After absorbing the heat, the high temperature pressure CO_2 enters into the turbine. After the work is done, the high temperature and low-pressure CO_2 enters into the hot sides of the regenerators to preheat the low temperature and high-pressure CO_2. Therefore, the working mediums in the cold side and hot side of PCHE as the regenerator in supercritical CO_2 Brayton cycle are low temperature and high-pressure supercritical CO_2 and high temperature and low-pressure supercritical CO_2, respectively. Referring to the parameters of low temperature regenerator in Mecheri and Le Moullec's research [34], the inlet pressure is 21 MPa and the inlet temperature is 373 K in the cold side, and the inlet pressure is 9 MPa and the inlet temperature is 493 K in the hot side in this study. The thermal physical properties of CO_2 used in this research are shown in Figure 4, which are calculated by the software NIST Refprop 9.1. It can be found that pressure has a great influence on the thermal properties of supercritical CO_2, and the thermal physical properties change dramatically when the temperature close to the pseudo-critical point. The mass flow rates in the cold and hot sides of PCHEs are always equal, and the mass flux range is 200–600 kg/m^2 s. The solid domain material is Alloy 617. All the thermal physical property data were input software by piecewise linear interpolation method.

Numerical method

The computational domain shown in Figure 2 and the whole process of the supercritical CO_2 heat transfer in PCHE is regarded as three-dimensional, incompressible, and quasi-steady. Therefore, the governing

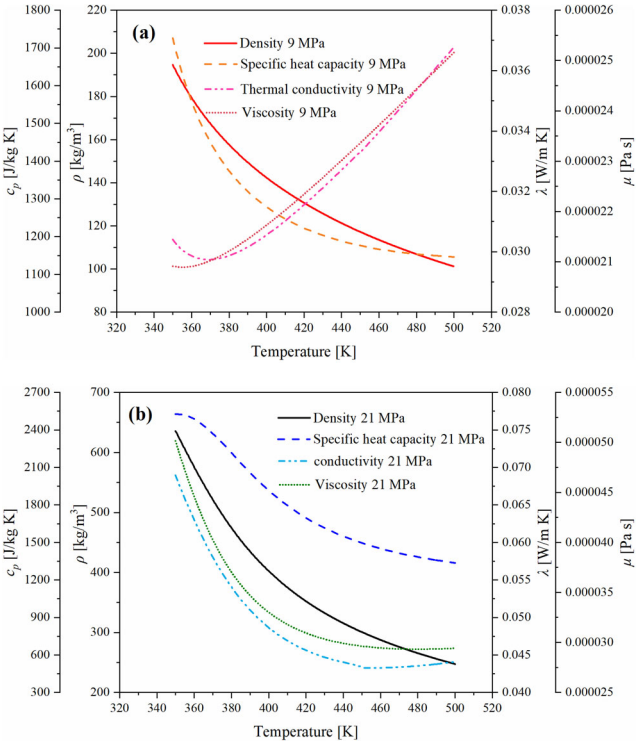


Figure 4. Thermal physical properties of supercritical CO_2 under different pressures used in this research.

equations of mass, momentum and energy can be respectively written in Cartesian tensor form as:

$$\frac{\partial(\rho v_j)}{\partial x_j} = 0 \tag{1}$$

$$\frac{\partial(\rho v_i v_j)}{\partial x_j} = -\frac{\partial p}{\partial x_j} + \rho g_i + \frac{\partial}{\partial x_j}\left[(\mu + \mu_t)\left(\frac{\partial v_i}{\partial x_j} + \frac{\partial v_j}{\partial x_i} - \frac{2}{3}\frac{\partial v_k}{\partial x_k}\right)\right] \tag{2}$$

$$\frac{\partial(\rho v_j H_e)}{\partial x_j} = \frac{\partial}{\partial x_j}\left[\left(\lambda + \frac{c_p \mu_t}{Pr_t}\right)\frac{\partial T}{\partial x_j}\right] \tag{3}$$

where ρ, v, p, g, μ, μ_t, H_e, λ, c_p, Pr_t, and T and represent the density, velocity, pressure, gravity acceleration, dynamic viscosity, turbulent viscosity, enthalpy, thermal conductivity, specific heat, turbulent Prandtl number, and temperature of the fluid, respectively.

The shear stress transfer (SST) k-ω turbulence model proposed by Menter [35] has high practicability and accuracy in the prediction of supercritical convection heat transfer characteristics and has been widely used in many previous numerical simulation studies of PCHEs. Therefore, the SST k-ω turbulence model was also adopted in this research. The transport equations for turbulent kinetic energy k and specific dissipation rate ω in SST k-ω turbulence model are written in Cartesian tensor form as:

$$\frac{\partial(\rho k v_i)}{\partial x_i} = \frac{\partial}{\partial x_j}\left(\Gamma_k \frac{\partial k}{\partial x_j}\right) + G_k - Y_k \tag{4}$$

$$\frac{\partial(\rho \omega v_i)}{\partial x_i} = \frac{\partial}{\partial x_j}\left(\Gamma_\omega \frac{\partial \omega}{\partial x_j}\right) + G_\omega - Y_\omega + D_\omega \tag{5}$$

where Γ is the effective diffusivity, G is the production term, Y is the dissipation term, D is the cross-diffusion term, respectively.

The CFD software ANSYS FLUENT 16.0 was used to calculate the conjugated heat transfer of supercritical CO_2. All inlet conditions are mass flow inlet, and outlet conditions are pressure outlet. Semi-implicit method for pressure linked equations-consistent (SIMPLEC) algorithm was adopted to solve the coupled equations of pressure and velocity. Second-order discretization scheme was used for pressure calculation, and the discretization of energy, momentum, turbulent kinetic energy, specific dissipation rate, and energy equations were all used the second order upwind scheme to improve the calculation accuracy. The under-relaxation factors were adjusted with the convergence of the calculation to ensure the convergence accuracy and speed. When the residuals of all equations are less than 10^{-5}, the calculated results are considered to converge.

In this paper, heat transfer and flow characteristics are discussed in detail, so some physical quantities are calculated and shown below. The convective heat transfer coefficient h was calculated with Equation (6):

$$h = \frac{q_w}{T_w - T_b} \tag{6}$$

where T_w is the average wall temperature, q_w is the wall heat flux, and T_b is the average bulk temperature of the cross-section:

$$T_b = \frac{\int v \rho c_p T dA}{\int v \rho c_p dA} \tag{7}$$

where A is the area. The wall heat flux q_w and wall temperature T_w were calculated by area-weighted average with the follow equation:

$$X_w = \frac{1}{A}\int X dA \tag{8}$$

X is the physical quantity being calculated. All the physical quantities can be obtained directly in Fluent.

The Nusselt number is defined in Equation (9):

$$Nu = \frac{h D_h}{\lambda_b} \tag{9}$$

where D_h is the hydraulic diameter of PCHE channel, and λ_b is the thermal conductivity of CO_2 when the temperature is T_b.

$$D_h = \frac{4A_c}{P} \tag{10}$$

where A_c is the cross-section area of PCHE channel, and P is the wetted perimeter of PCHE channel.

The Fanning friction factor f can be calculated as:

$$f = \frac{\Delta p D_h}{2v_b^2 \rho_b L_\alpha} = \frac{\Delta p D_h \rho_b}{2M^2 L_\alpha} \tag{11}$$

where Δp is the pressure drop, v_b is the average bulk velocity, ρ_b is the density of CO_2 when the temperature is T_b, M is the mass flux, and L_α is the flow length of channel:

$$L_\alpha = \frac{L}{\cos\alpha} \tag{12}$$

Grid independence study and validation of the numerical results

The software ANSYS ICEM CFD was adopted in this study for meshing. In order to solve the equations accurately, the near-wall mesh is encrypted. The height of the first layer mesh near the wall is controlled to ensure the dimensionless wall distance $y^+ < 1$ under all working conditions to ensure the flow characteristic in the viscous sublayer can be captured [36]. The mesh structures are generally shown in Figure 5. In order to verify the mesh independence, the PCHE model when $\alpha = 15°$ and $s = 0$ mm was taken as an example to calculate the pressure drops and the temperature difference between the inlet and outlet in the cold and hot sides at a mass flux of 400 kg/m^2 s by using 5 sets of grids as shown in Table 2. Obviously, it can be seen from Figure 6 that Grid 3 of 2,194,305 nodes is accurate enough in the calculation. For other different models, the nodes density and distribution of the meshes follow the same law.

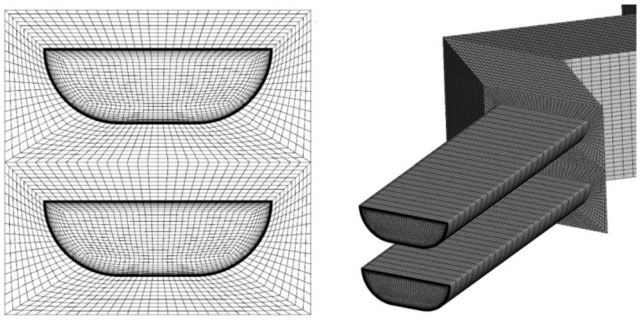


Figure 5. Mesh of PCHE when $\alpha = 15°$ and $s = 0.8$ mm.

There is no experimental data of supercritical CO_2 flow and heat transfer in PCHE under the similar model and working conditions in this paper. Geometrical structure and working conditions have great influence on the flow and heat transfer of PCHE, so there is no widely applicable empirical correlation at present. Two typical heat transfer empirical correlations [17, 37] of zigzag PCHEs in Table 3 were used to calculate the Nusselt number, and then compared the values calculated by CFD. The results are shown in Figure 7, and there are large errors between CFD simulation and empirical correlation calculation.

In order to verify the correctness of the numerical method in this study, the experimental process of Ishizuka's experiment [19] is calculated by the numerical model in this work, and the numerical results compared with the experimental data. As shown in Table 4, the experimental data of temperature difference in the cold side and the hot side agree well with the numerical calculation, and the errors are 1.27% and 1.47%, respectively. The numerical calculation of

Table 2. The grid number sets of PCHE when $\alpha = 15°$ and $s = 0$ mm.

Gird	Number
Grid 1	1,217,321
Grid 2	1,640,259
Grid 3	2,194,305
Grid 4	2,810,406
Grid 5	3,711,671

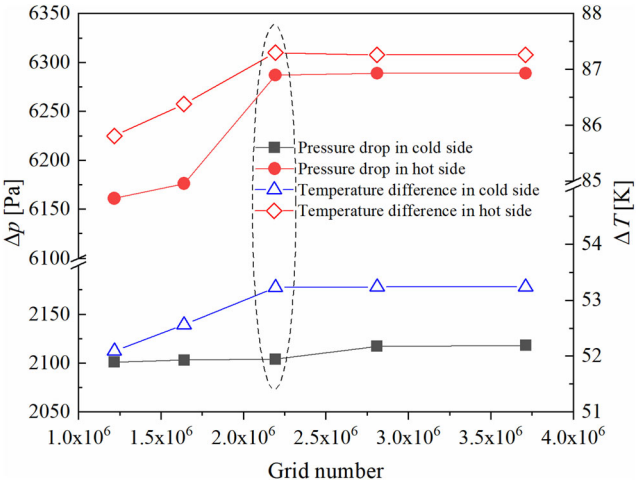


Figure 6. Test of grid independence about PCHE when $\alpha = 15°$ and $s = 0$ mm.

Table 3. Typical heat transfer empirical correlations of zigzag PCHEs.

Reference	Empirical correlation
Ngo et al. [17]	$Nu = (0.1696 \pm 0.0144) Re^{0.629 \pm 0.009} Pr^{0.317 \pm 0.014}$
Kim et al. [37]	$Nu = (0.292 \pm 0.0015) Re^{0.8138 \pm 0.005}$

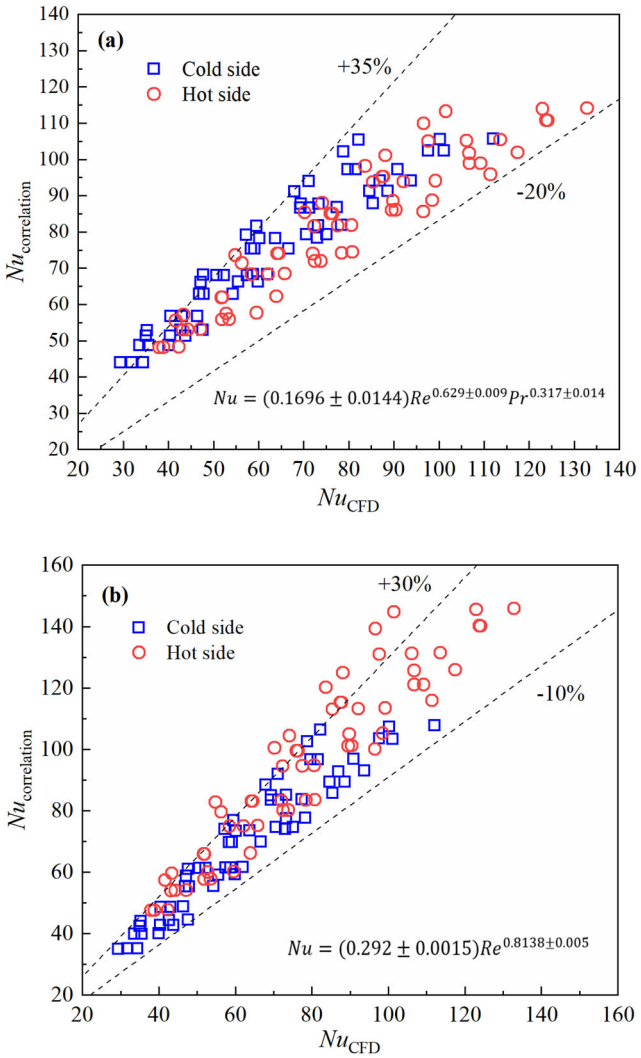


Figure 7. Comparison of *Nu* numbers obtained from CFD simulation and empirical correlations [17, 37].

the pressure drop in the cold side is in good agreement with the experiment, and the error is only 0.56%. However, the error of pressure drop in the hot side between the experiment and numerical calculation is 7.96%, which may be due to the influence of model simplification [32]. Therefore, the numerical model in this paper is effective and acceptable.

Results and discussion

Effect of channel width on heat transfer

Heat transfer rate per unit volume is an important index of compact heat exchanger, so the influence of zigzag channel width on heat transfer rate per unit volume of PCHE is studied. As shown in Figure 8, the heat transfer per unit volume of the same PCHE increases with the increase of mass flux. The heat transfer rates per unit volume of PCHEs with different bending angles all increase with the increase of channel width at the same mass flux. For example, the heat transfer rates per unit volume of $s = 2.4$ mm increased by 31.73% compared with that of $s = 0$ mm when the bending angle $\alpha = 25°$ and mass flux is 200 kg/m^2 s. It is worth noting that, the increments of heat transfer rate per unit volume of all PCHEs become gentle with the increase of channel width at the same mass flux. Obviously, there is a limit to this increment, and the bending angle is smaller, it reaches the limit more easily.

Table 4. Numerical results compared with experimental data [19].

Parameters	Experimental data	Numerical results	Error
Cold channel pressure difference [Pa]	73,220	73,261	0.56%
Hot channel pressure difference [Pa]	24,180	22,256	7.96%
Cold channel temperature difference [K]	140.38	138.6	1.27%
Hot channel temperature difference [K]	169.6	172.1	1.47%

In order to further analyze the influence of channel width on heat transfer, Figures 9 and 10 show the change of Nusselt number in the cold side and hot side of PCHE, respectively. Figure 9 shows the change of Nusselt number in the cold side of PCHE with the mass flux. The Nusselt number in the cold side of the same PCHE increases with the increase of mass flux. As shown in Figure 9b,c, when the bending angle α is equal to 20° and 25°, the Nusselt number in the cold side of PCHE increases with the increase of channel width at the same mass flux. As shown in Figure 9a, when the bending angle $\alpha = 15°$ and the mass flux $\leq$300 kg/m^2 s, the Nusselt number also shows the above change. However, when the mass flux is greater than 300 kg/m^2 s, with the increase of channel width, the Nusselt number increases first, then decreases and increases last, presenting a wave change. On the whole, the heat transfer of PCHE in the cold side is enhanced when the width of the channel is increased, especially when the bending angle $\alpha = 20°$ and the mass flux is 600 kg/m^2 s, the Nusselt number of $s = 2.4$ mm increases by 36.7% compared with that of $s = 0$ mm.

Figure 10 shows the change of Nusselt number in the hot side of PCHE with the mass flux. The Nusselt number in the hot side of the same PCHE increases with the increase of mass flux. As shown in Figure 10a, when the bending angle $\alpha = 15°$ and the mass flux is 300 kg/m^2 s, the Nusselt number increases firstly and then decreases with the increase of the channel width, while shows wave variation in the case of other mass flux. As shown in Figure 9b, when the bending angle $\alpha = 20°$ and the mass flux is 200 kg/m^2 s, the Nusselt number increases with the increase of

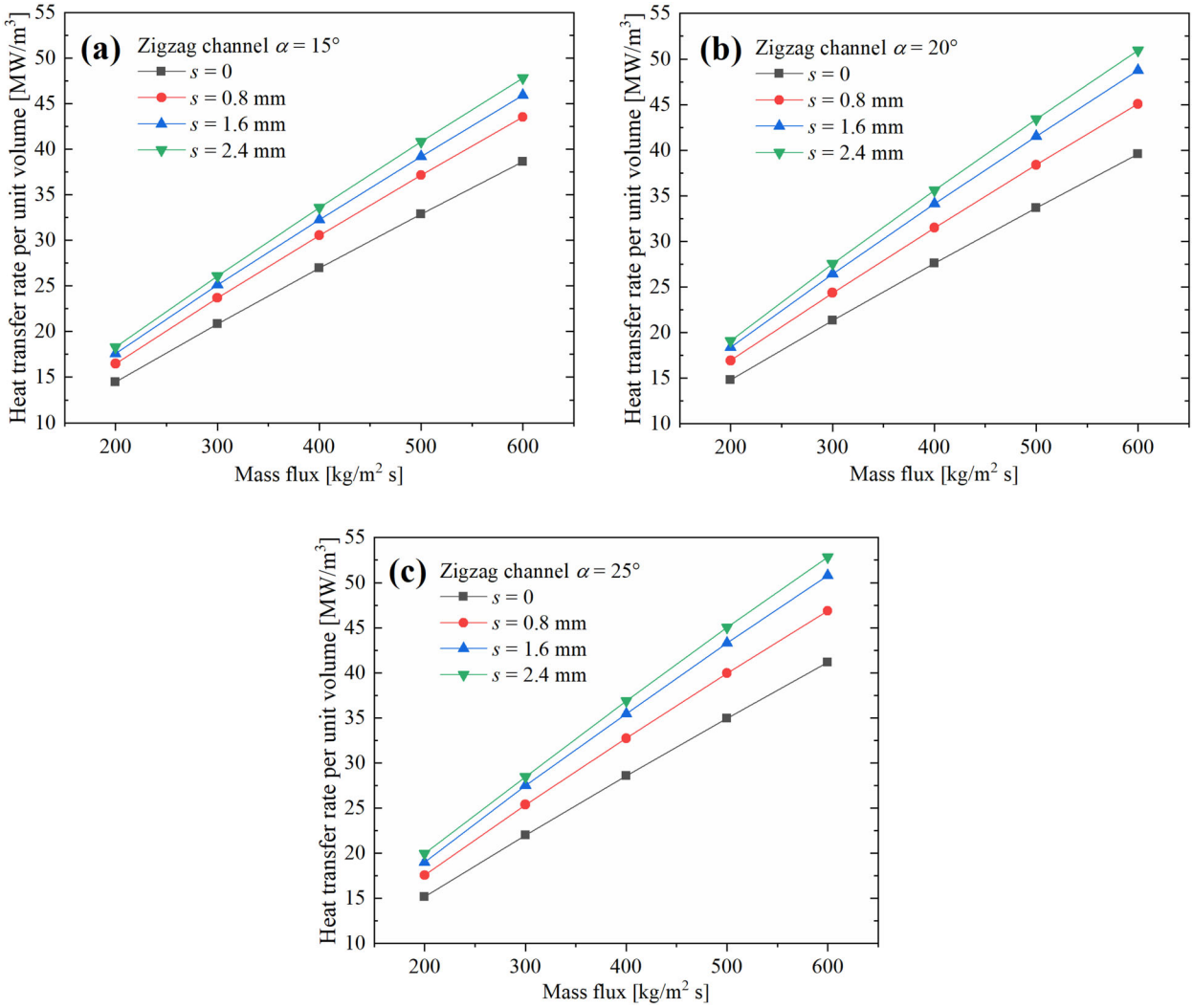


Figure 8. Variation of heat transfer rate per unit volume with mass flux.

channel width at the same mass flux. When the mass flux $\geq$300 kg/m^2 s, the Nusselt number increases firstly and then decreases with the channel width. However, the Nusselt numbers of $s = 1.6$ mm and $s = 2.4$ mm are always close no matter how the mass flux changes. As shown in Figure 10c, when the bending angle $\alpha = 25°$, the Nusselt number of the PCHE in the hot side increases with the increase of the channel width at the same mass flux. On the whole, the heat transfer of PCHE in the hot side is enhanced when the width of the channel is increased. In addition, this heat transfer enhancement is the most significant when the bending angle $\alpha = 20°$. For example, the Nusselt number of $s = 1.6$ mm is 41.5% larger than that of $s = 0$ mm when the mass flux is 600 kg/m^2 s in the hot side of PCHE.

It can be concluded from the above analysis that increasing channel width can enhance heat transfer generally, and part of the reason may be that the cross-sectional area and heat transfer area of the channel are increased. However, PCHEs with the bending angle $\alpha = 15°$ have the most complicated heat transfer behavior. The possible reason is that the bending angle, channel width and mass flux all affect the heat transfer. When the bending angle is small, the change of mass flux and channel width does not have a great influence on the absolute value of Nu number, indicating that none of the effects on heat transfer plays a particularly significant leading role. At this time, these factors are coupled together to cause the complexity of heat transfer.

Effect of channel width on friction factor

Most studies on structure optimization of PCHE hope to enhance heat transfer and reduce the friction factor. Therefore, the friction factor of channel is one of the important parameters of PCHE performance index. In this paper, the influence of channel width

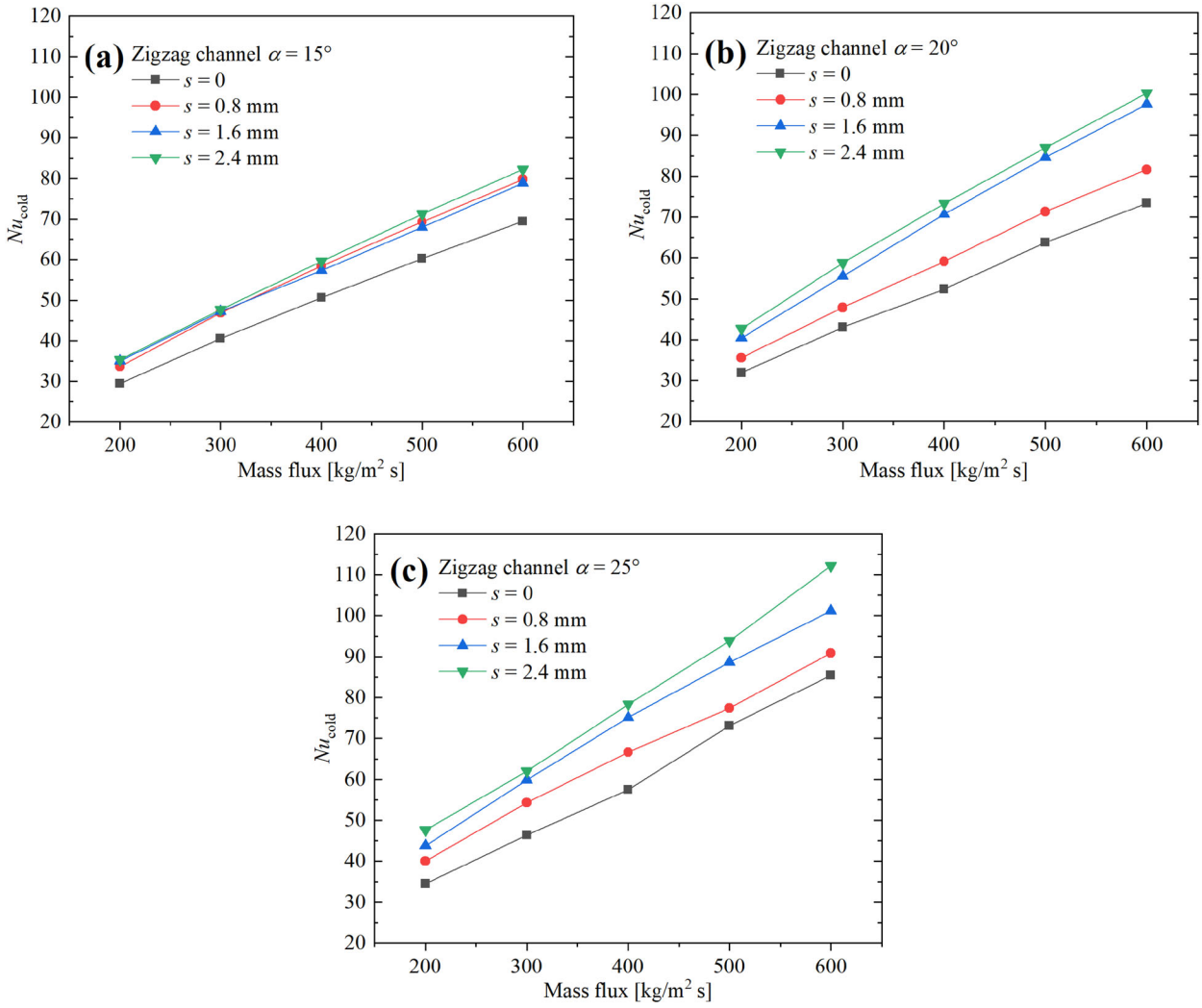


Figure 9. Variation of Nusselt number with mass flux in the cold side of PCHE.

variation on the friction factor of PCHE in both cold and hot sides is analyzed in detail.

Figure 11 shows the change of friction factor in the cold side of PCHE with the mass flux. Obviously, the influence of channel width of PCHE on friction factor is different with different channel bending angles. As shown in Figure 11a, when the bending angle $\alpha = 15°$, the friction factor of the same PCHE decreases with the increase of mass flux, and the friction factor decreases firstly and then increases with the increase of channel width at the same mass flux. As shown in Figure 11b, when the bending angle $\alpha = 20°$, the friction factor of the same PCHE decreases with the increase of mass flux. When the mass flux $\leq$300 kg/m^2 s, the friction factor decreases firstly and then increases with the increase of channel width. When the mass flux $\geq$400 kg/m^2 s, the friction factor increases with the increase of channel width. As shown in Figure 11c, the friction factor increases with the increase of channel width at the same mass flux. When $s = 0$ mm and $s = 0.8$ mm, the friction factor of the same PCHE decreases with the increase of mass flux. When $s = 1.6$ mm, the friction factor of the same PCHE decreases firstly and then increases with the increase of mass flux. When $s = 2.4$ mm, the friction factor of the same PCHE increases firstly, then decreases and increases last with the increase of mass flux to showing wave variation.

Figure 12 shows the change of friction factor in the hot side of PCHE with the mass flux. As shown in Figure 12, friction factors in the same PCHE all decrease with the increase of mass flux. As shown in Figure 11a, the friction factor decreases firstly and then increases with the increase of channel width at the same mass flux. As shown in Figure 12b, when the mass flux is 200 kg/m^2 s, the friction factor firstly decreases and then increases with the increase of channel width, while the friction factor increases with the increase of channel width under the condition of other mass flux. As shown in Figure 12c, friction

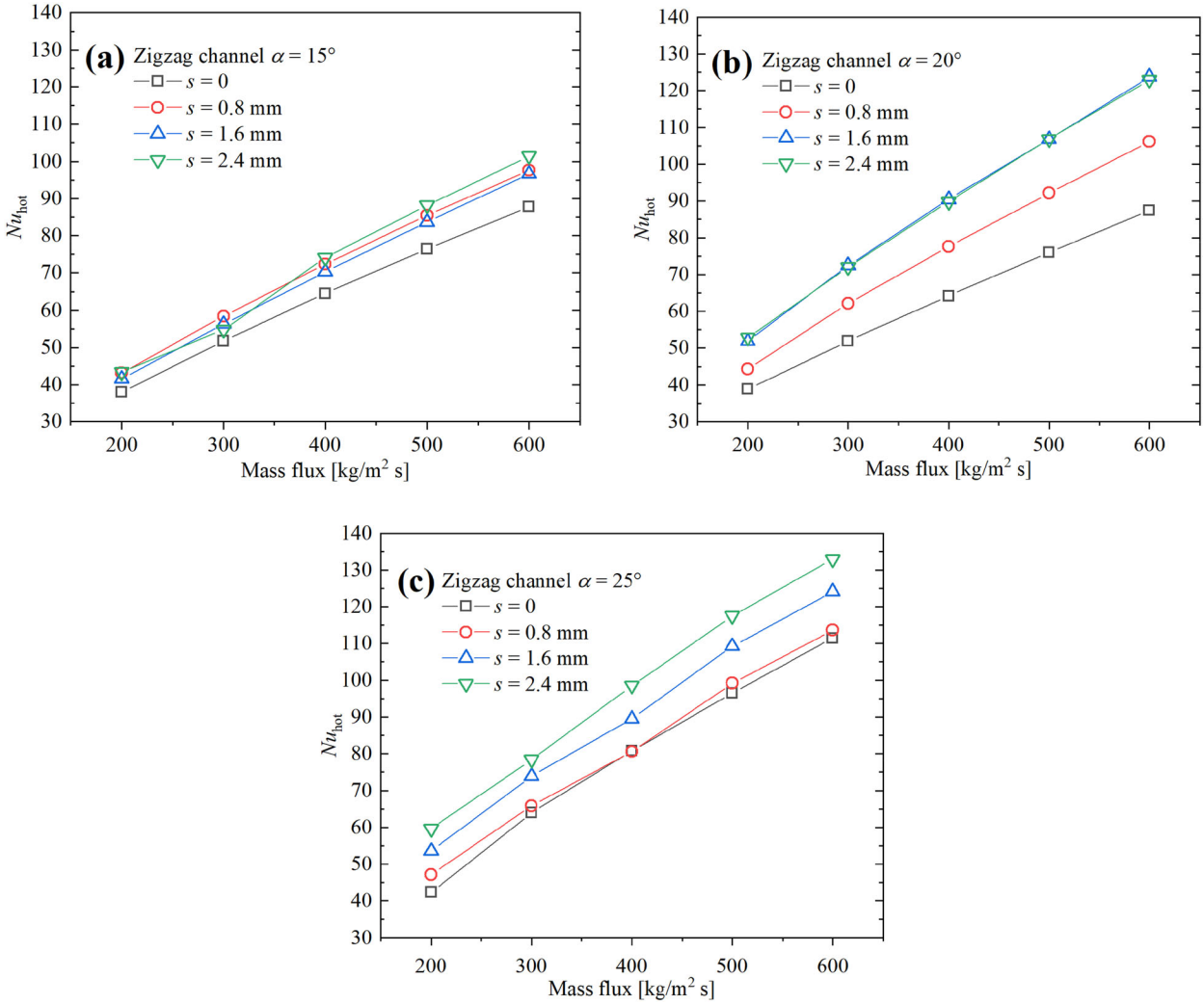


Figure 10. Variation of Nusselt number with mass flux in the hot side of PCHE.

factors all increase with the increase of channel width. In particular, when bending angles α is 20° and 25°, the friction factors increase significantly of $s = 2.4$ mm.

The influence of channel width variation on friction factor of PCHE at different bending angles is complex from the above analysis. In general, when the bending angle $\alpha = 15°$, increasing the channel width within a certain range can effectively reduce the friction factor in both cold side and hot side. Compared with the semicircular section, the friction factor of the arcuate section in the cold side and hot side can be reduced by 5.75% and 7.25%, respectively. However, this reduction has a limit, and it will increase the friction factor to a certain extent if the channel width is increased beyond the limit. When the bending angle $\alpha = 20°$, increasing the channel width within a certain range can also reduce the friction factor under low mass flux. When the bending angle $\alpha = 25°$, increasing the width of the channel basically increases the friction factor, and the friction coefficient increases sharply in particular when $s = 2.4$ mm.

Flow and heat transfer characteristics analysis

In order to further understand the performance of flow and heat transfer caused by the change of channel width, a detailed analysis of flow and heat transfer characteristics in the channel are conducted in this section. The pitch 2 in the hot side of PCHEs is used as analysis object, and a series of sections are established along the flow direction.

Figure 13 shows the temperature distribution in cross-sections when the mass flux is 400 kg/m^2 s. As shown in Figure 12a, when the bending angle $\alpha = 15°$, there are obviously and relatively regular high temperature regions in all sections from 2-1 to 3-1 along the flow direction, and the temperature distributions in the cross-sections do not change much along the way but oscillate slightly with the change of channel

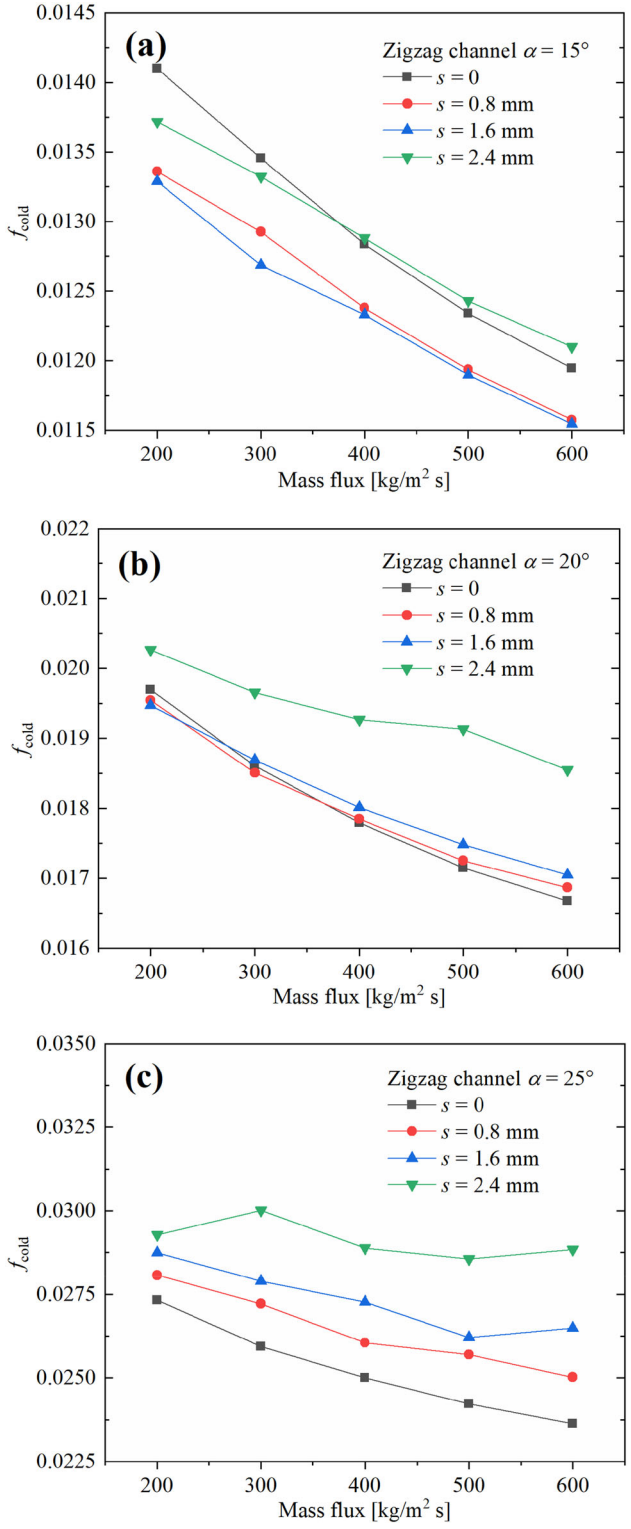


Figure 11. Variation of friction factor with mass flux in the cold side of PCHE.

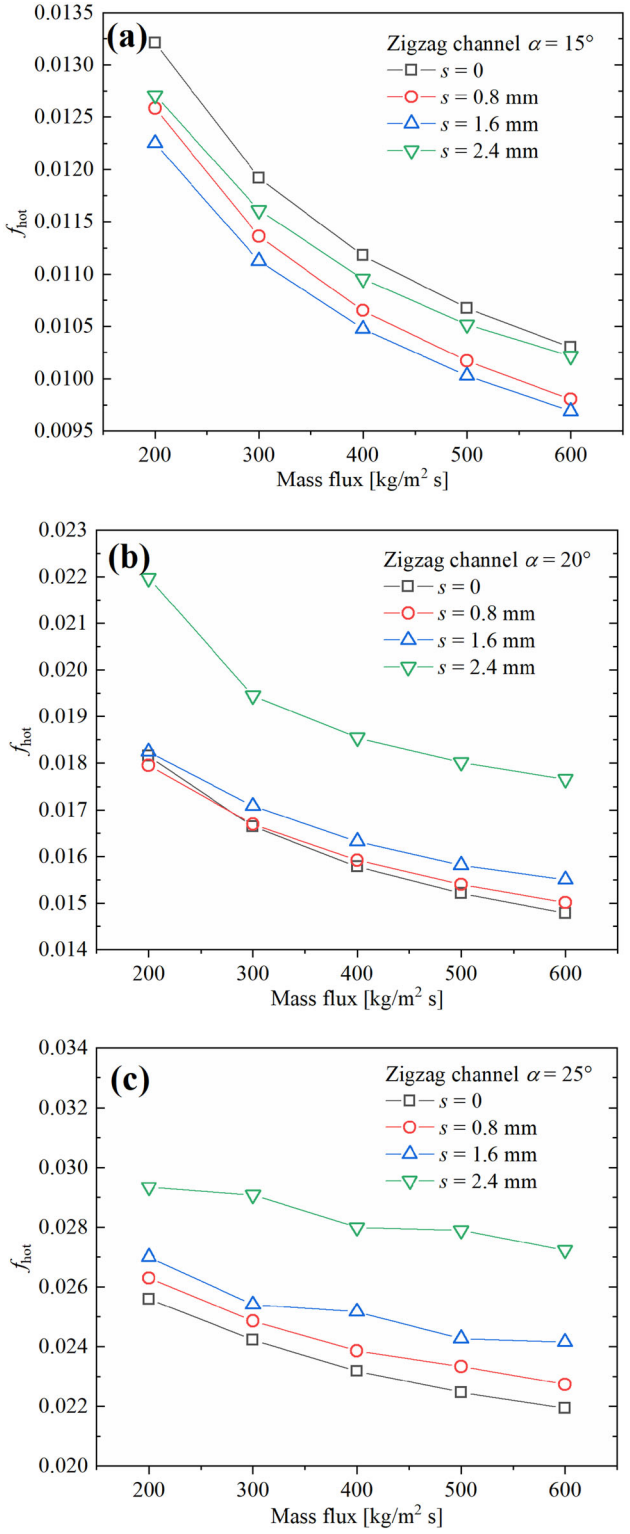
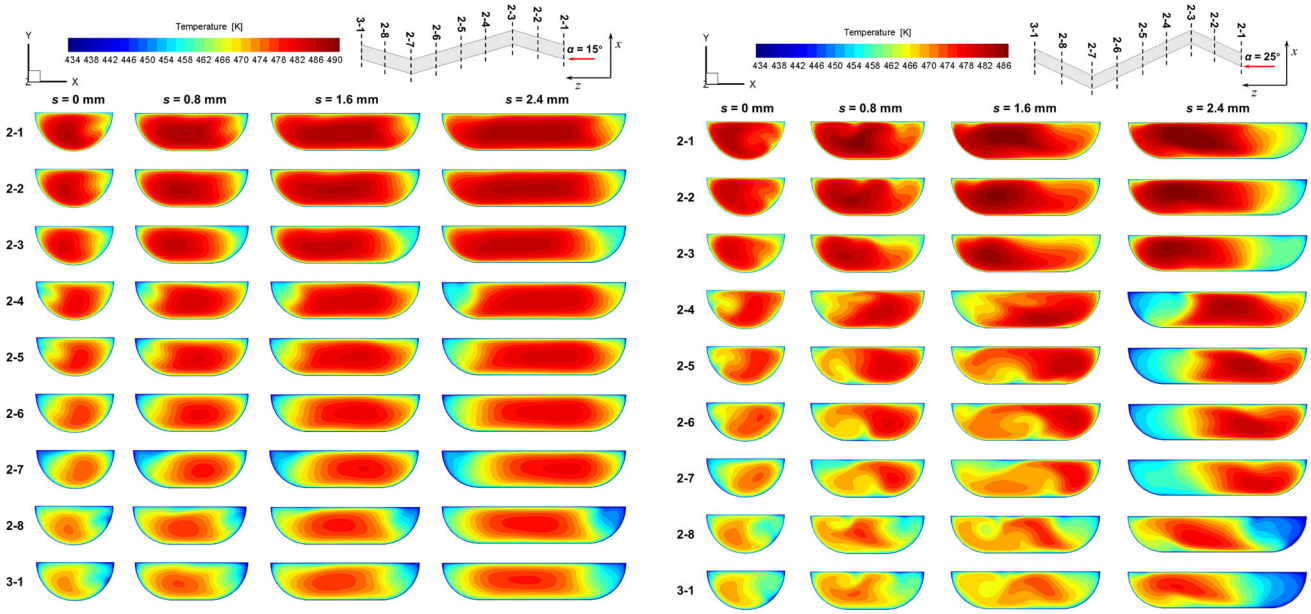


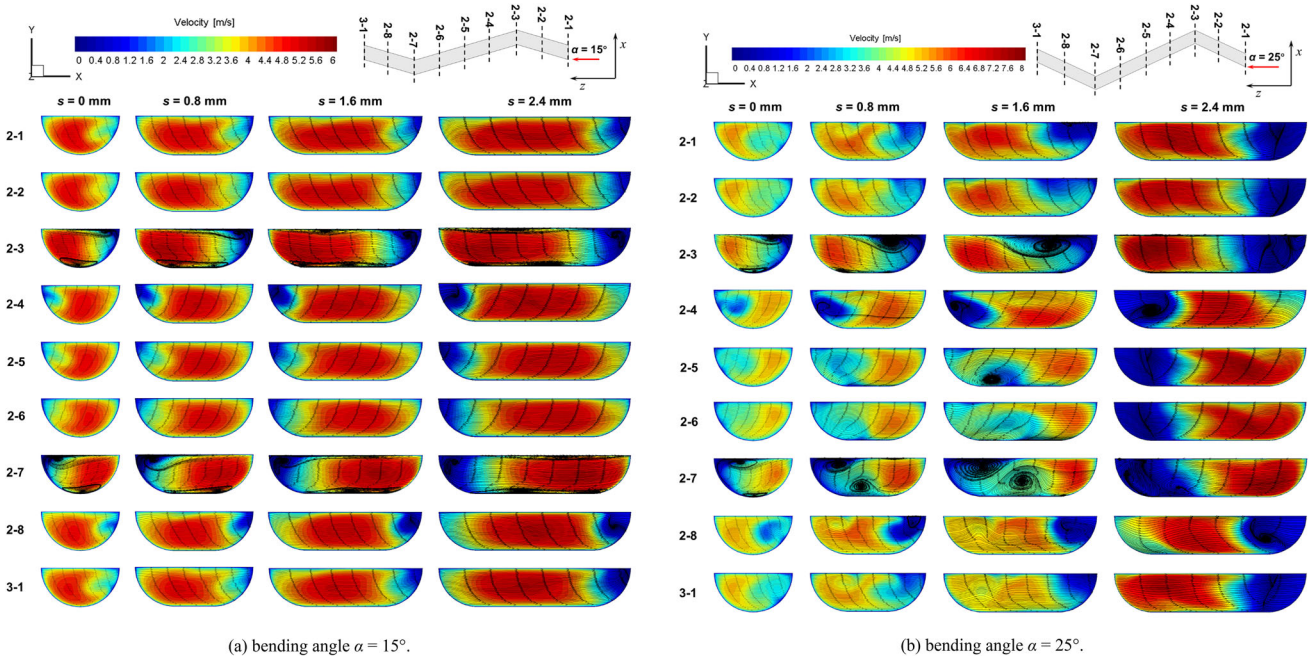
Figure 12. Variation of friction factor with mass flux in the hot side of PCHE.

direction. The temperatures near the sharp corner of the upper wall of all channels are lower, which are the heat transfer enhancement areas. When the width of the channel increases, the temperature distribution characteristics in the cross-sections at the same position are not very different, especially for the three groups of arcuate sections from $s = 0.8$ mm to $s = 2.4$ mm. This is obviously corresponding to Figure 9a, that is, the overall Nusselt number in the hot side does not change much from $s = 0.8$ mm to $s = 2.4$ mm.



(a) bending angle $\alpha = 15°$. (b) bending angle $\alpha = 25°$.

Figure 13. Temperature distribution in the cross-sections of pitch 2 when the mass flux is 400 kg/m^2 s in the hot side.



(a) bending angle $\alpha = 15°$. (b) bending angle $\alpha = 25°$.

Figure 14. Velocity distributions and streamlines in cross-sections of pitch 2 when the mass flux is 400 kg/m^2 s in the hot side.

As shown in Figure 13b, when the bending angle $\alpha = 25°$, the temperature distributions in the cross-sections along the flow direction change dramatically. The temperature dispersions in the cross-sections increase significantly with the increase of channel width, especially when $s = 2.4$ mm, there are even clear temperature separations between the left and right in the channels. The increase of bending angle makes the overall Nusselt number increase for the same PCHE channel width in Figure 10, and this heat transfer enhancement effect is more significant for wide channels ($s \geq 0.8$ mm). Comparing Figure 13a with Figure 13b, it can be found that with the increase of bending angle, the changes of temperature dispersions in the

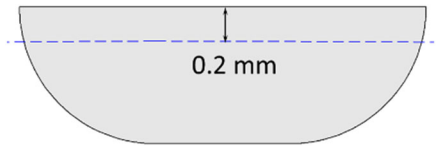
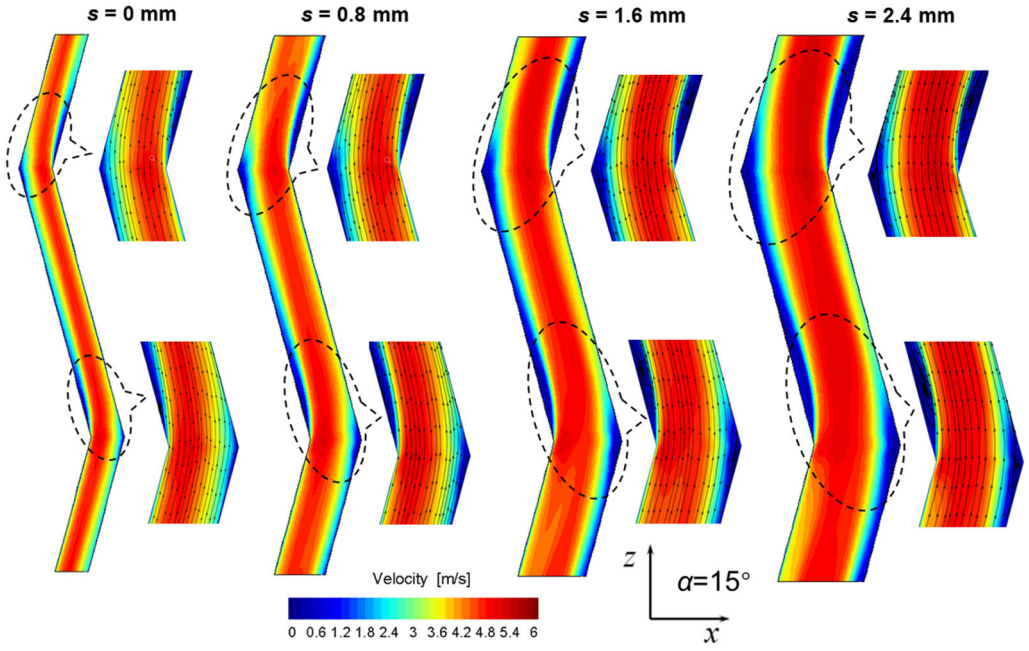
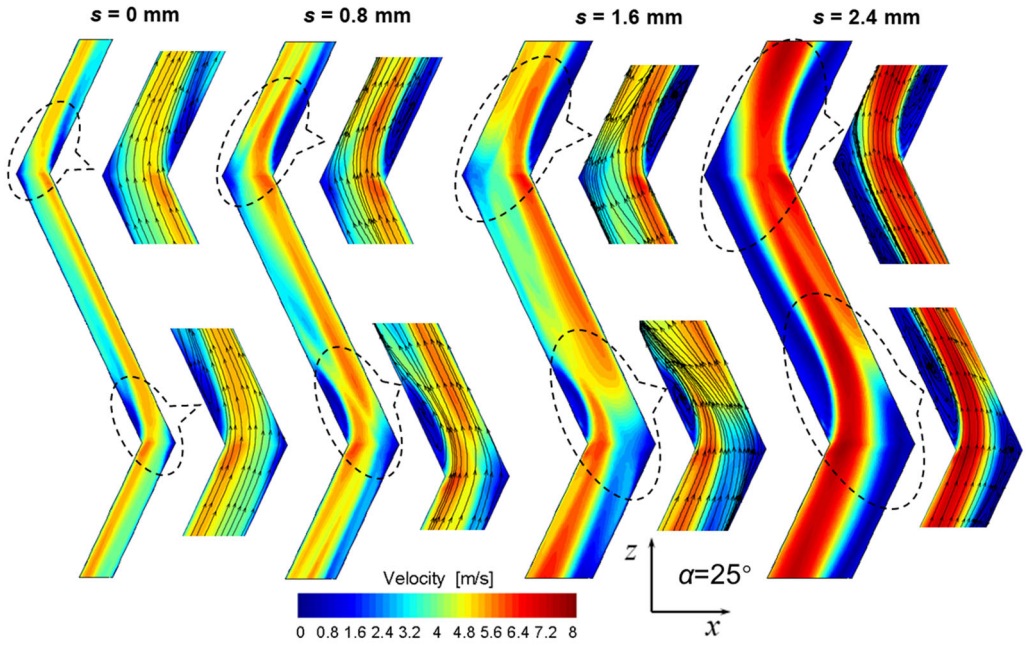


Figure 15. Horizontal section position.



(a) bending angle $\alpha = 15°$.



(b) bending angle $\alpha = 25°$.

Figure 16. Velocity distributions and streamlines in horizontal sections of pitch 2 when the mass flux is 400 kg/m^2 s in the hot side.

cross-sections for the wide channel ($s \geq 0.8$ mm) are obviously much more obvious than that for the narrow channel ($s = 0$ mm), which can initially explain the phenomenon mentioned above in Figure 10.

The velocity distributions and streamlines in cross-sections when the mass flux is 400 kg/m^2 s are shown in Figure 14. As shown in Figure 14a, when the bending angle $\alpha = 15°$, the velocity distributions in all cross-sections don't change much from 2-1 to 3-1 along the flow direction. Similar to the temperature distributions in Figure 13a, there are regular central regions of high velocity in the cross-section obviously, which also oscillate with the change of channel direction. Upper and lower vortices appear of the

secondary flows in all cross-sections at positions 2-3 and 2-7. These positions are channel bends; therefore, these vortices are Dean vortices generated by centrifugal force when the direction of fluid flow changes.

As shown in Figure 14b, when the bending angle $\alpha = 25°$, the velocity distributions are much more complicated obviously. In general, the proportion of low-speed zone in the cross-section increases with the increase of channel width at the same position. When $s \leq 1.6$ mm, Dean vortices appear at positions 2-3 and 2-7 in all cross-sections, and the scale of vortices increases with the increase of width. However, when $s = 2.4$ mm, it can be found that the velocity distributions between the left and right sides in the cross-sections are significantly divided, and a large flow stagnation area appears. Therefore, the streamlines at positions 2-3 and 2-7 are markedly different from those at other widths.

In order to further analyze the influence of velocity changes, horizontal sections parallel to the flow direction were made at a distance of 0.2 mm from the upper wall of the channels as shown in Figure 15. Figure 16 shows the velocity distributions and streamlines in horizontal sections of pitch 2 when the mass flux is 400 kg/m^2 s. As shown in Figure 16a, all channels have high-velocity zones flow regions occupying the main part of the cross-sections when the bending angle $\alpha = 15°$. There are low-velocity zones near the left and right walls. The reason for this phenomenon is that the channel corner makes the fluid impact the windward side, and the flow separation occurs on the leeward side. With the increase of channel width, flow impact and separation become more and more significant, resulting in reverse flow and vortex phenomenon. Especially, when $s = 2.4$ mm, the low-velocity zone generated by flow impact and the low-velocity zone generated by flow separation are mixed together and occupy an important part in the whole flow region. The proportion of low-velocity zones would undoubtedly affect the flow resistance of the whole region. This can explain why the friction factors decrease firstly and then increase as the channel widths increase in Figure 12b.

When the bending angle $\alpha = 25°$, as shown in Figure 16b, the phenomenon of flow impact and separation is much more significant than that of small angle. Especially when $s = 2.4$ mm, the low-velocity area and the high-velocity area are almost evenly divided. Obviously, flow impact and separation make major contributions to the flow resistance. This can explain why the friction factors increase with increasing width, and the increases are particularly significant when $s = 2.4$ mm in Figure 12c.

The above analysis shows that bending angle causes flow impact and separation in the channel, and these phenomena become more significant with the increase of bending angle. Flow impact and separation can enhance the heat transfer and flow resistance together. However, narrow channel width can inhibit the flow impact and separation. Therefore, the effect of bending angle and channel width on flow and heat transfer is strongly coupled.

Conclusions

In this study, a series of zigzag PCHE models with different arcuate-sectional widths and bending angles was established, and three-dimensional numerical calculation method was used to analysis the heat transfer and flow characteristics of supercritical CO_2 in PCHEs under different mass flux. Through the discussion, the main conclusions are as follows:

1. When the channel width is increased, the heat transfer rate per unit volume of the zigzag PCHE is enhanced, and the maximum growth of arcuate section is 31.73% than semicircular section. However, this enhancement has a certain limit, and the bending angle is smaller, it reaches the limit more easily. The heat transfer on both sides of the zigzag PCHE will be enhanced with the increase of channel width on the whole. Compared with the semicircular section, the maximum enhancement of *Nu* number of the arcuate section in the cold side and hot sides is 36.7% and 41.5%, respectively. However, when the bending angle $\alpha = 15°$, the *Nu* number varies complexly with the channel width increasing in both sides. The coupled interaction of channel width, bending angle and mass flux in zigzag PCHE results in the complexity of heat transfer.
2. The influence of channel width variation on friction factor of zigzag PCHE at different bending angles is complex. In general, when the bending angle $\alpha \leq 20°$, increasing the channel width within a certain range can effectively reduce the friction factor in both cold side and hot side. Compared with the semicircular section, the friction factor of the arcuate section in the cold side and hot side can be reduced by 5.75% and 7.25%, respectively. However, this reduction has a limit, and it will increase the friction factor if the channel width is increased beyond the limit and flow flux is above a certain range. When the bending angle $\alpha \geq 20°$, increasing the width of the channel basically

increases the friction factor, and the friction coefficient increases sharply in particular when $s = 2.4$ mm. The above phenomena are closely related to the flow impact and separation in the zigzag channel.

3. Bending angle causes flow impact and separation in the zigzag channel, and these phenomena become more significant with the increase of bending angle. Flow impact and separation can enhance the heat transfer and flow resistance together. However, narrow channel width can inhibit the flow impact and separation. The coupling of bending angle, channel width and mass flux makes the change of heat transfer and friction factor complicated.
4. In the past, in order to enhance the heat transfer of zigzag PCHE, the bending angle was usually increased, but this also brought an increase in flow resistance. Through the study of this paper, it is found that increasing the width of the channel at a certain angle cannot only reduce the resistance coefficient, but also enhance the heat transfer. This has certain significance for the design optimization of PCHE structure.

Disclosure statement

No potential conflict of interest was reported by the author(s).

Funding

This work was supported by the National Natural Science Foundation of China (Grant Nos. U20B2035 & 11675128).

Notes on contributors



Qingqing Wang is a Ph.D. candidate in State Key Laboratory of Multiphase Flow in Power Engineering, Xi'an Jiaotong University, Xi'an, China. His current research fields are supercritical heat transfer experiment and numerical calculation, compact heat exchanger design and nuclear reactor safety.



Xin Huang is a Ph.D. candidate in State Key Laboratory of Multiphase Flow in Power Engineering, Xi'an Jiaotong University, Xi'an, China. His current research fields are supercritical heat transfer experiment and numerical calculation, and flow field analysis of air-cooling power plant.



Bo Xu is a Ph.D. candidate in State Key Laboratory of Multiphase Flow in Power Engineering, Xi'an Jiaotong University, Xi'an, China. His current research fields are air-liquid two-phase flow in nuclear piping, and flow noise analysis.



Qiuxiang Chen is a Ph.D. candidate in State Key Laboratory of Multiphase Flow in Power Engineering, Xi'an Jiaotong University, Xi'an, China. Her current major research field is nuclear reactor safety, including analysis of nuclear reactor water-loss accident, and nuclear reactor direct safety injection.



Haijun Wang is a full professor in State Key Laboratory of Multiphase Flow in Power Engineering, Xi'an Jiaotong University, Xi'an, China. He obtained his Ph.D. in power engineering and engineering thermophysics in 2001 from Xi'an Jiaotong University. His research interests include multiphase heat transfer, supercritical heat transfer, nuclear reactor safety and air-cooling system.

References

[1] G. Liu, Y. Huang, J. Wang, and R. Liu, "A review on the thermal-hydraulic performance and optimization of printed circuit heat exchangers for supercritical CO_2 in advanced nuclear power systems," *Renew. Sustain. Energy Rev.*, vol. 133, p. 110290, Nov. 2020. DOI: 10.1016/j.rser.2020.110290.

[2] M. Saeed, A. S. Berrouk, M. S. Siddiqui, and A. A. Awais, "Numerical investigation of thermal and hydraulic characteristics of sCO_2-water printed circuit heat exchangers with zigzag channels," *Energy Convers. Manag.*, vol. 224, p. 113375, Sep. 2020. DOI: 10.1016/j.enconman.2020.113375.

[3] T. Cong, Z. Wang, R. Zhang, B. Wang, and Y. Zhu, "Thermal-hydraulic performance of a PCHE with sodium and sCO_2 as working fluids," *Ann. Nucl. Energy*, vol. 157, p. 108210, Jul. 2021. DOI: 10.1016/j.anucene.2021.108210.

[4] W.-X. Chu, X.-H. Li, T. Ma, Y.-T. Chen, and Q.-W. Wang, "Experimental investigation on SCO_2-water heat transfer characteristics in a printed circuit heat exchanger with straight channels," *Int. J. Heat Mass Transf.*, vol. 113, pp. 184–194, Oct. 2017. DOI: 10.1016/j.ijheatmasstransfer.2017.05.059.

[5] C. Huang *et al.*, "Review on the characteristics of flow and heat transfer in printed circuit heat exchangers," *Appl. Therm. Eng.*, vol. 153, pp. 190–205, May 2019. DOI: 10.1016/j.applthermaleng.2019.02.131.

[6] H. Wang, S. Wang, J. Zhang, J. Wang, and Y. Huang, "Direct numerical simulation of the turbulent flow and heat transfer of supercritical CO_2 in a semicircular pipe," *Int. J. Heat Mass Transf.*, vol. 168, p. 120882, Apr. 2021. DOI: 10.1016/j.ijheatmasstransfer.2020.120882.

[7] M. Chen, X. Sun, and R. N. Christensen, "Thermal-hydraulic performance of printed circuit heat exchangers with zigzag flow channels," *Int. J. Heat Mass Transf.*, vol. 130, pp. 356–367, Mar. 2019. DOI: 10.1016/j.ijheatmasstransfer.2018.10.031.

[8] J.-W. Seo, Y.-H. Kim, D. Kim, Y.-D. Choi, and K.-J. Lee, "Heat transfer and pressure drop characteristics in straight microchannel of printed circuit heat exchangers," *Entropy*, vol. 17, no. 5, pp. 3438–3457, 2015. DOI: 10.3390/e17053438.

[9] Z. Ren, C.-R. Zhao, P.-X. Jiang, and H.-L. Bo, "Investigation on local convection heat transfer of supercritical CO_2 during cooling in horizontal semicircular channels of printed circuit heat exchanger," *Appl. Therm. Eng.*, vol. 157, p. 113697, Jul. 2019. DOI: 10.1016/j.applthermaleng.2019.04.107.

[10] J. H. Park *et al.*, "Experimental study of a straight channel printed circuit heat exchanger on supercritical CO_2 near the critical point with water cooling," *Int. J. Heat Mass Transf.*, vol. 150, p. 119364, Apr. 2020. DOI: 10.1016/j.ijheatmasstransfer.2020.119364.

[11] T. Ma, L. Li, X.-Y. Xu, Y.-T. Chen, and Q.-W. Wang, "Study on local thermal–hydraulic performance and optimization of zigzag-type printed circuit heat exchanger at high temperature," *Energy Convers. Manag.*, vol. 104, pp. 55–66, Nov. 2015. DOI: 10.1016/j.enconman.2015.03.016.

[12] Z. Ren, L. Zhang, C.-R. Zhao, P.-X. Jiang, and H.-L. Bo, "Local flow and heat transfer of supercritical CO_2 in semicircular zigzag channels of printed circuit heat exchanger during cooling," *Heat Transf. Eng.*, vol. 42, no. 22, pp. 1889–1913, 2021. DOI: 10.1080/01457632.2020.1834205.

[13] R. C. Alvarez, A. P. C. Sarmiento, L. H. R. Cisterna, F. H. Milanese, and M. B. H. Mantelli, "Heat transfer investigation of a 90° zigzag channel diffusion-bonded heat exchanger," *Appl. Therm. Eng.*, vol. 190, p. 116823, May 2021. DOI: 10.1016/j.applthermaleng.2021.116823.

[14] W. Chu, X. Li, Y. Chen, Q. Wang, and T. Ma, "Experimental study on small Scale printed circuit heat exchanger with zigzag channels," *Heat Transf. Eng.*, vol. 42, no. 9, pp. 723–735, 2021. DOI: 10.1080/01457632.2020.1735779.

[15] Z.-X. Wen, Y.-G. Lv, Q. Li, and P. Zhou, "Numerical study on heat transfer behavior of wavy channel supercritical CO_2 printed circuit heat exchangers with different amplitude and wavelength parameters," *Int. J. Heat Mass Transf.*, vol. 147, p. 118922, Feb. 2020. DOI: 10.1016/j.ijheatmasstransfer.2019.118922.

[16] Q. Jing and D. Zhang, "Numerical study of flow structure and thermohydraulic performance of SCO_2 in S-shaped printed circuit exchanger with longitudinal ribs," *Heat Transf. Res.*, vol. 51, no. 2, pp. 147–171, 2020. DOI: 10.1615/HeatTransRes.2019028340.

[17] T. L. Ngo, Y. Kato, K. Nikitin, and T. Ishizuka, "Heat transfer and pressure drop correlations of microchannel heat exchangers with S-shaped and zigzag fins for carbon dioxide cycles," *Exp. Therm. Fluid Sci.*, vol. 32, no. 2, pp. 560–570, 2007. DOI: 10.1016/j.expthermflusci.2007.06.006.

[18] J.-W. Zhao, R. Zhao, Y.-L. Nian, and W.-L. Chen, "Experimental study of supercritical CO_2 in a vertical adaptive flow path heat exchanger," *Appl. Therm. Eng.*, vol. 188, p. 116597, Apr. 2021. DOI: 10.1016/j.applthermaleng.2021.116597.

[19] D. E. Kim, M. H. Kim, J. E. Cha, and S. O. Kim, "Numerical investigation on thermal-hydraulic performance of new printed circuit heat exchanger model," *Nucl. Eng. Des.*, vol. 238, no. 12, pp. 3269–3276, 2008. DOI: 10.1016/j.nucengdes.2008.08.002.

[20] W.-X. Chu, K. Bennett, J. Cheng, Y.-T. Chen, and Q.-W. Wang, "Thermo-hydraulic performance of printed circuit heat exchanger with different cambered airfoil fins," *Heat Transf. Eng.*, vol. 41, no. 8, pp. 708–722, 2020. DOI: 10.1080/01457632.2018.1564203.

[21] C.-Y. Zhu, Y. Guo, H.-Q. Yang, B. Ding, and X.-Y. Duan, "Investigation of the flow and heat transfer characteristics of helium gas in printed circuit heat exchangers with asymmetrical airfoil fins," *Appl. Therm. Eng.*, vol. 186, p. 116478, Mar. 2021. DOI: 10.1016/j.applthermaleng.2020.116478.

[22] S. K. Mylavarapu *et al.*, "Fabrication and design aspects of high-temperature compact diffusion bonded heat exchangers," *Nucl. Eng. Des.*, vol. 249, pp. 49–56, Aug. 2012. DOI: 10.1016/j.nucengdes.2011.08.043.

[23] H. Zhang, J. Guo, X. Huai, X. Cui, and K. Cheng, "Buoyancy effects on coupled heat transfer of supercritical pressure CO_2 in horizontal semicircular channels," *Int. J. Heat Mass Transf.*, vol. 134, pp. 437–449, May 2019. DOI: 10.1016/j.ijheatmasstransfer.2019.01.045.

[24] M. Saeed and M.-H. Kim, "Thermal and hydraulic performance of SCO_2 PCHE with different fin configurations," *Appl. Therm. Eng.*, vol. 127, pp. 975–985, Dec. 2017. DOI: 10.1016/j.applthermaleng.2017.08.113.

[25] R. de la Torre, J.-L. François, and C.-X. Lin, "Optimization and heat transfer correlations development of zigzag channel printed circuit heat exchangers with helium fluids at high temperature," *Int. J. Therm. Sci.*, vol. 160, p. 106645, Feb. 2021. DOI: 10.1016/j.ijthermalsci.2020.106645.

[26] S. Baik, S. G. Kim, J. Lee, and J. I. Lee, "Study on CO_2–water printed circuit heat exchanger performance operating under various CO_2 phases for S-CO_2 power cycle application," *Appl. Therm. Eng.*, vol. 113, pp. 1536–1546, Feb. 2017. DOI: 10.1016/j.applthermaleng.2016.11.132.

[27] Z.-X. Wen, Y.-G. Lv, and Q. Li, "Comparative study on flow and heat transfer characteristics of sinusoidal and zigzag channel printed circuit heat exchangers," *Sci. China Technol. Sci.*, vol. 63, no. 4, pp. 655–667, 2020. DOI: 10.1007/s11431-019-1492-2.

[28] S. Y. Lee, B. G. Park, and J. T. Chung, "Numerical studies on thermal hydraulic performance of zigzag-type printed circuit heat exchanger with inserted straight channels," *Appl. Therm. Eng.*, vol. 123, pp. 1434–1443, Feb. 2017. DOI: 10.1016/j.applthermaleng.2017.05.198.

[29] A. M. Aneesh, A. Sharma, A. Srivastava, and P. Chaudhury, "Effects of wavy channel configurations on thermal-hydraulic characteristics of Printed Circuit Heat Exchanger (PCHE)," *Int. J. Heat Mass Transf.*, vol. 118, pp. 304–315, Mar. 2018. DOI: 10.1016/j.ijheatmasstransfer.2017.10.111.

[30] S.-M. Lee and K.-Y. Kim, "Comparative study on performance of a zigzag printed circuit heat exchanger with various channel shapes and configurations," *Heat Mass Transf.*, vol. 49, no. 7, pp. 1021–1028, 2013. DOI: 10.1007/s00231-013-1149-4.

[31] S. Jeon, Y.-J. Baik, C. Byon, and W. Kim, "Thermal performance of heterogeneous PCHE for supercritical CO_2 energy cycle," *Int. J. Heat Mass Transf.*, vol. 102, pp. 867–876, Nov. 2016. DOI: 10.1016/j.ijheatmasstransfer.2016.06.091.

[32] Y. Yang *et al.*, "Investigation on the effects of narrowed channel cross-sections on the heat transfer performance of a wavy-channeled PCHE," *Int. J. Heat Mass Transf.*, vol. 135, pp. 33–43, Jun. 2019. DOI: 10.1016/j.ijheatmasstransfer.2019.01.044.

[33] J. Lao, Q. Fu, W. Wang, J. Ding, and J. Lu, "Heat transfer characteristics of printed circuit heat exchanger with supercritical carbon dioxide and molten salt," *J. Therm. Sci.*, vol. 30, no. 3, pp. 880–891, 2021. DOI: 10.1007/s11630-020-1374-3.

[34] M. Mecheri and Y. L. Moullec, "Supercritical CO_2 Brayton cycles for coal-fired power plants," *Energy*, vol. 103, pp. 758–771, May 2016. DOI: 10.1016/j.energy.2016.02.111.

[35] F. R. Menter, "Two-equation eddy-viscosity turbulence models for engineering applications," *AIAA J.*, vol. 32, no. 8, pp. 1598–1605, 1994. DOI: 10.2514/3.12149.

[36] Z. Li *et al.*, "Orientation effect in helical coils with smooth and rib-roughened wall: Toward improved gas heaters for supercritical carbon dioxide Rankine cycles," *Energy*, vol. 140, no. part 1, pp. 530–545, Dec. 2017. DOI: 10.1016/j.energy.2017.09.010.

[37] S. G. Kim, Y. Lee, Y. Ahn, and J. I. Lee, "CFD aided approach to design printed circuit heat exchangers for supercritical CO_2 Brayton cycle application," *Ann. Nucl. Energy*, vol. 92, pp. 175–185, Jun. 2016. DOI: 10.1016/j.anucene.2016.01.019.